Force transmission in migrating cells

Maxime F. Fournier,[1] Roger Sauser,[1] Davide Ambrosi,[2] Jean-Jacques Meister,[1] and Alexander B. Verkhovsky[1]

[1]Laboratoire de Biophysique Cellulaire, Ecole Polytechnique Fédérale de Lausanne, CH-1015 Lausanne, Switzerland
[2]Dipartimento di Matematica, Politecnico di Milano, 20133 Milano, Italy

During cell migration, forces generated by the actin cytoskeleton are transmitted through adhesion complexes to the substrate. To investigate the mechanism of force generation and transmission, we analyzed the relationship between actin network velocity and traction forces at the substrate in a model system of persistently migrating fish epidermal keratocytes. Front and lateral sides of the cell exhibited much stronger coupling between actin motion and traction forces than the trailing cell body. Further analysis of the traction–velocity relationship suggested that the force transmission mechanisms were different in different cell regions: at the front, traction was generated by a gripping of the actin network to the substrate, whereas at the sides and back, it was produced by the network's slipping over the substrate. Treatment with inhibitors of the actin–myosin system demonstrated that the cell body translocation could be powered by either of the two different processes, actomyosin contraction or actin assembly, with the former associated with significantly larger traction forces than the latter.

Introduction

During cell migration, forces developed in the actin microfilament system are transmitted to the substrate to drive cell motion. The major force-generating reactions in the cytoskeleton are believed to be the assembly of actin filaments and their interaction with the motor protein myosin II (Mitchison and Cramer, 1996; Mogilner and Oster, 2003; Ridley et al., 2003). Actin assembly is thought to drive protrusion at the leading edge of the cell (Pantaloni et al., 2001; Mogilner and Oster, 2003; Pollard and Borisy, 2003). In contrast, the role of myosin II is controversial. By analogy to skeletal muscle, it was argued that interaction between actin and myosin filaments generates contractile forces that pull the cell body forward and promote retraction at the back of the cell (Maciver, 1996; Verkhovsky et al., 1999). However, multiple studies demonstrated that the motor activity of myosin II isn't required for cell migration (Wessels et al., 1988; Lombardi et al., 2007). Instead, it was suggested that myosin II plays a role in the establishment of cell polarity and in the coordination between different cell domains (Csucs et al., 2007, Lombardi et al., 2007; Yam et al., 2007; Vicente-Manzanares et al., 2008). Part of the traction forces applied by the cell to the substrate depends on myosin activity (Jurado et al., 2005; Beningo et al., 2006), but there are also indications that traction forces at the front are myosin independent (Iwadate and Yumura, 2008) and that myosin influences the organization of force pattern rather than the magnitude of the forces (Lo et al., 2004; Lombardi et al., 2007).

The transmission of traction forces involves complexes of adhesion proteins that connect actin filaments to the extracellular matrix (Geiger and Bershadsky, 2002; Chen et al., 2004). Recent studies demonstrated that this connection is not rigid but rather involves multiple points of slippage where relative movement of the connection chain's links can occur (Hu et al., 2007; Wang, 2007). It is not clear what role slippage plays in force transmission and how it influences migration efficiency. A widely accepted hypothesis likened cell adhesion to a clutch (Heidemann and Buxbaum, 1998; Smilenov et al., 1999), implying that when the clutch is engaged, there is no slippage between the cytoskeleton and the substrate and productive movement of the cell can occur. When the clutch is disengaged, polymerization pressure at the membrane interface and myosin-dependent contraction cause actin to slip back, resulting in the phenomenon known as retrograde flow (Cramer, 1997), but the cell does not move. Thus, the clutch hypothesis implies that the less the actin network moves with respect to the substrate, the more effectively it transmits the traction force. However, retrograde flow occurs during migration as well as in the resting cells (Jurado et al., 2005;

Correspondence to Maxime F. Fournier: maxime.fournier@epfl.ch

The Rockefeller University Press $30.00
J. Cell Biol. Vol. 188 No. 2 287–297
www.jcb.org/cgi/doi/10.1083/jcb.200906139

Schaub et al., 2007; Yam et al., 2007), and the rate of flow does not always inversely correlate with the cell velocity (Theriot and Mitchison, 1992), suggesting that viscous friction between the actin network and the substrate could be an intrinsic part of the force transmission mechanism. A viscous friction mechanism would imply that traction forces are directly proportional to the velocity of actin motion, a theory which is opposite to the assumption of the clutch hypothesis. Recently, Gardel et al. (2008) reported a biphasic relationship between actin flow and traction stress in epithelial cells: at low actin velocities, traction stress directly correlated to the velocity, and at higher velocities, it was inversely correlated. These authors concluded that the force transmission mechanism can switch between two different modes and that the switch is controlled by actin velocity (with a switching point at ∼10 nm/s). Recent study of neuronal cells (Chan and Odde, 2008) also suggested two different modes of the adhesive machinery: the switching between load and fail dynamics and frictional slippage depended in this case on the rigidity of the substrate. The role of the different modes of adhesion and putative switches between them in the overall mechanism of cell migration isn't clear yet.

To understand the role of actin flow and myosin activity and the physical principles of the force transmission mechanism in the context of cell migration, it is beneficial to look at a model system with simple and predictable motile behavior. Fish epidermal keratocytes represent a favorable model because of their fast and persistent migration and simple and stable shape (Lee et al., 1993). Cytoskeletal dynamics and the distribution of traction forces in keratocytes were previously analyzed in separate studies (Svitkina et al., 1997; Galbraith and Sheetz, 1999; Oliver et al., 1999; Doyle and Lee, 2002; Schaub et al., 2007) but not correlated to each other. The overall mechanism of keratocyte migration remains controversial. Different models explain keratocyte migration either in terms of contraction of actin–myosin fibers (Anderson et al., 1996; Oliver et al., 1999; Anderson and Cross, 2000) and a network (Verkhovsky et al., 1999; Schaub et al., 2007) or in terms of the balance between actin assembly and membrane tension (Keren et al., 2008). In this study, we use a keratocyte system to correlate actin dynamics and traction forces over the whole cell, to map the efficiency of force transmission, and to reveal slipping and gripping mechanisms differentially involved in stress transmission in different parts of the cell. We also investigate contributions of actin assembly and myosin-dependent contractility to force generation and provide evidence that cell translocation could be powered by two different engines.

Results

Simultaneous observation of actin dynamics and substrate deformation

To investigate how the dynamics of the cytoskeleton correlate with the forces exerted by the cell on the substrate, we simultaneously observed actin flow and substrate deformation during the migration of fish epidermal keratocytes (Fig. 1 A and Video 1). The pattern of actin flow in the cells moving on elastic gelatin substrata (Doyle and Lee, 2002) was similar to that previously observed on a rigid glass substrate (Schaub et al., 2007). A kymograph demonstrated a slow retrograde flow of actin associated with backward deformation of the substrate at the front of the cell (Fig. 1 B) and fast anterograde motion of actin concomitant with a very slow forward displacement of the substrate at the back of the cell (Fig. 1 C). At the sides of the cell, actin moved toward the cell center, and the substrate was deformed in the same direction (Fig. 1 D). Near the cell margin, the motion of the substrate switched abruptly from a centripetal to a centrifugal direction (Fig. 1 D, arrowheads), suggesting a release and elastic recoil of the substrate after the passage of the cell.

In summary, substrate was continuously displaced in the direction of actin motion under all regions of the cell. However, the movement of the substrate was slower than that of the actin filaments, indicating that force transmission involved slippage of the components of the actin cytoskeleton with respect to the substrate.

Comparison of the maps of actin velocity and substrate stress

Next, we generated two-dimensional maps of actin velocity and substrate stress. An actin velocity map produced on gelatin substrata (Fig. 2 A) was similar to one previously obtained on glass substrate (Schaub et al., 2007). We applied the algorithm previously used to track actin motion (Schaub et al., 2007) to the movement of fluorescent beads incorporated into the substrate and obtained the map of substrate velocity. The pattern of substrate velocity under the cell was similar to that of actin velocity, but substrate velocity was ∼10 times smaller than actin velocity (Fig. 2 B). Subtracting substrate velocity from actin velocity yielded the map of actin velocity with respect to the substrate (Fig. 2 C). This map was similar to the actin velocity map in laboratory coordinates (Fig. 2 A), which was expected, given the small values of substrate velocity.

A traction vector map (Fig. 2 E) was computed based on the substrate deformation field (Fig. 2 D) using the finite element algorithm (Ambrosi, 2006). The traction map was consistent with one previously obtained by Doyle and Lee (2002). We observed backward-oriented traction forces on the substrate under the entire front of the cell and forward-oriented forces under the back of the cell. Backward-oriented forces on the substrate imply that equivalent forward-oriented forces are applied to the cell and vice versa. Therefore, forces under the front of the cell are propulsive (contributing to the cell's forward motion), whereas forces under the back resist this motion. The strongest forces were observed locally under the sides of the cell. These forces were oriented from the side toward the cell center and slightly forward, suggesting that traction at lateral regions had a component that resisted forward motion of the cell. The magnitude of traction stress varied in different cell regions and among different cells, but the variation was generally within the range that was previously reported (Oliver et al., 1999).

To investigate the relationship between actin motion and the traction stress, we compared the direction of stress with that of actin velocity. Fig. 2 F shows the map of the cosine of the

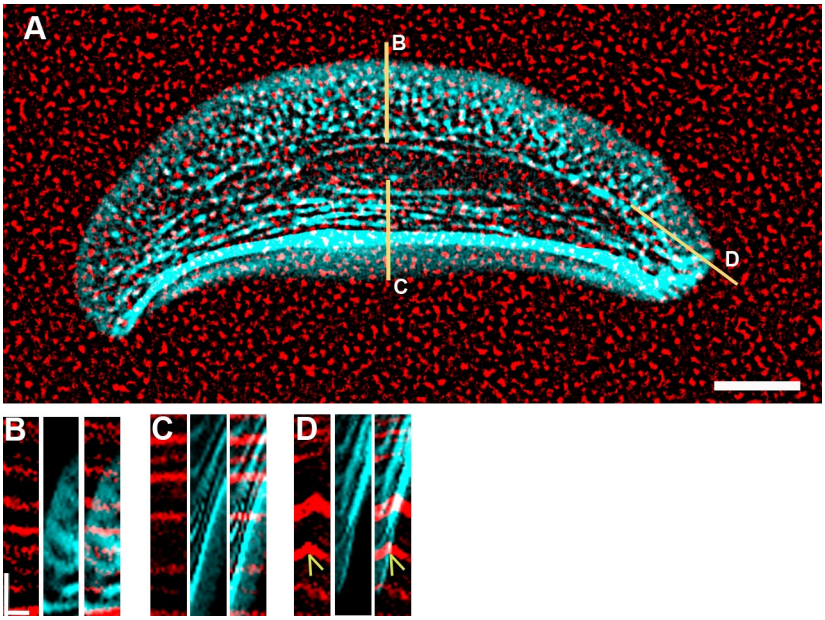

Figure 1. **Simultaneous observation of actin motion and substrate deformation in migrating keratocytes.** (A) The image of phalloidin-labeled actin (cyan) is superimposed on the image of the fluorescent beads (red) spread on the substrate surface (Video 1). (B–D) Kymographs generated along the lines labeled with B, C, and D in A. In each group of kymographs, the order of presentation from left to right is substrate (red), actin (cyan), and a merger of the two. The arrowheads in D indicate the change of bead motion direction corresponding to the release of the substrate at the lateral margin of the cell. For the kymograph: vertical bar, 10 μm; horizontal bar, 20 s. Bar, 10 μm.

angle between the vectors of stress and actin velocity at every cell location. Most of the cell areas exhibited close directional correlation between stress and actin velocity (Fig. 2 F, red area). At the front of the cell, both actin velocity and traction stress were oriented backward, at the back of the cell, the common orientation was forward, and at the cell sides, it was oriented toward its center. However, in the central region of the cell, the direction of actin motion was opposite to that of stress (Fig. 2 F, blue area). The values of actin velocity and stress in this region were small, but the opposite orientation of the stress and velocity was significant because it was consistently observed in all studied cells. This region was contained between the boundary where actin velocity changed from retrograde at the front of the cell to anterograde at its back and the boundary where stress orientation changed from backward to forward. Note that there was no contradiction between the apparent colinearity of actin and substrate motion and the opposite direction of stress in this region of the cell. The actin network moved forward concomitant with a slower motion of the substrate in the same direction, but the substrate still retained an overall backward deformation, which reflected a backward-directed stress.

Considering that motion of the actin network is transmitted through the adhesion machinery to the substrate, resulting in traction forces, the coupling between the actin network and the substrate could be characterized by a ratio of traction stress to the velocity of actin filaments with respect to the substrate. We termed this quantity the "coupling coefficient" (between traction stress at the substrate and actin motion). In terms of the clutch hypothesis, the coupling coefficient is a measure of engagement of the clutch. In terms of frictional slippage between the actin network and the substrate, the coupling coefficient could be considered an effective friction coefficient of the entire cytoskeleton–substrate connection, including possible multiple levels of slippage between different components of the force transmission chain. Frictional interpretation is only valid in the regions of the cell where the directions of actin velocity and the stress coincide (outside of the darkened region in Fig. 2, F and G). Even in these regions, the coupling coefficient may reflect various physical phenomena because the interaction of the actin network with the substrate may be not entirely frictional (see the next section). Nevertheless, this parameter is useful for illustrating different relationships between actin dynamics and traction in different regions of the cell.

We produced dynamic maps of the coupling coefficient over the entire cell based on double fluorescent video sequences of actin motion and substrate deformation. All maps (representative examples shown in Fig. 2, G and H) generally demonstrated a tight coupling between actin motion and traction throughout the region under the lamellipodia and the sides of the cell. In some cells, the coupling coefficient was maximal in the central region of the lamellipodia and gradually diminished toward the cell sides, with low coupling at the lateral rear extremities (Fig. 2 G), whereas other cells exhibited coupling that increased from the cell center to the sides, including the lateral rear corners (Fig. 2 H). In all cases, the cell body exhibited a significantly lower coupling coefficient than the front and the sides. These results suggest that both the lamellipodia and the sides of the cell are relatively strongly connected to the substrate and exert propulsive and resisting forces, whereas the cell body plays a less significant role in force transmission.

Our observations also suggested that the coupling coefficient may be a reliable indicator of changes of cell behavior. In steadily migrating cells, coupling maps were relatively stable with time (unpublished data). In the cell that changed direction during observation, we analyzed the relationship between the turning of the cell and changes of the coupling coefficient at the cell sides (Fig. 2, H and I; and Video 2). The coupling coefficient was initially distributed slightly asymmetrically (Fig. 2 H, top left; higher actin–substrate coupling at the cell's left). The cell then detached at the right and rotated to the left, concomitant with a further increase in the asymmetry of the coupling distribution. Subsequently, the cell continued to

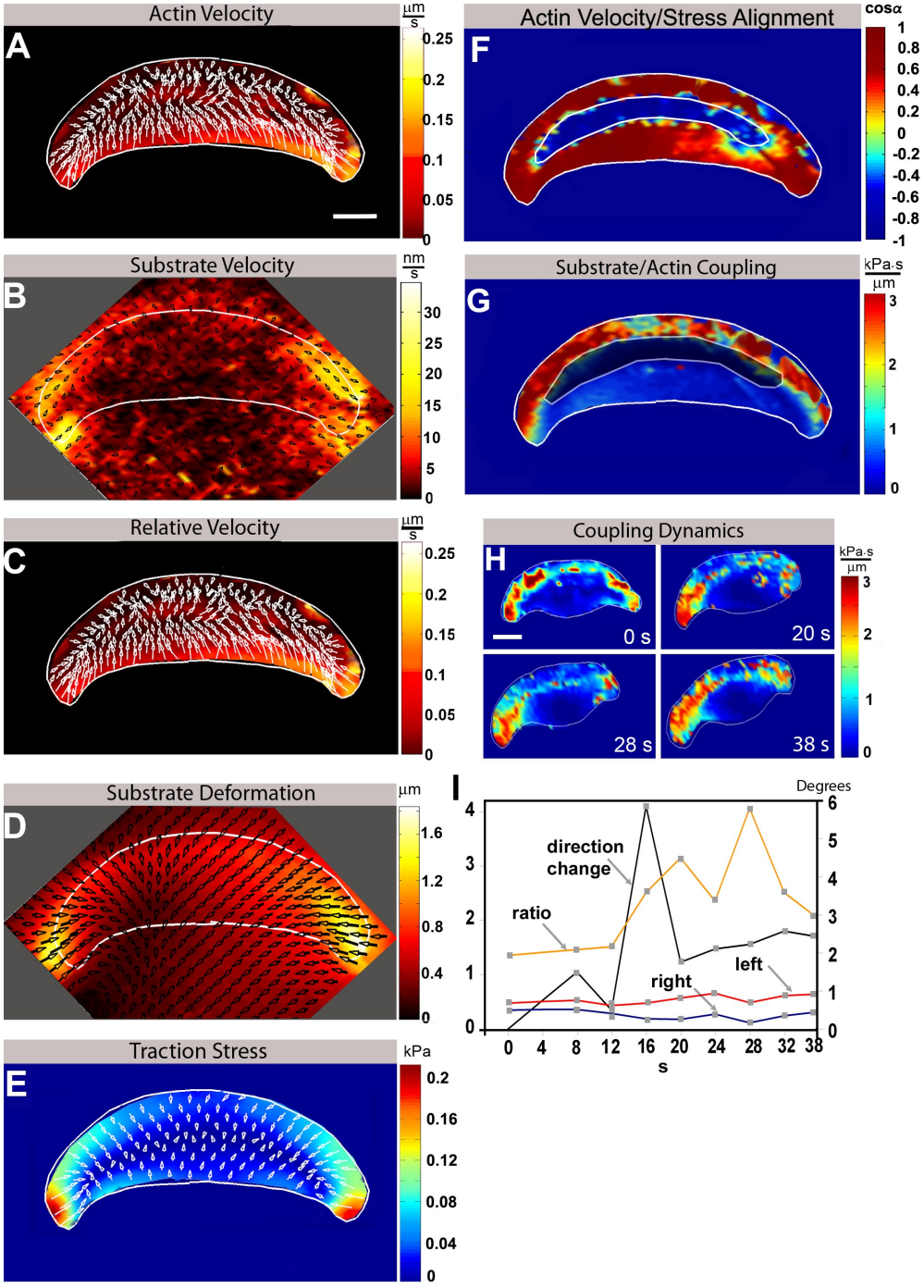

Figure 2. **Comparative mapping of actin velocity and substrate stress and computation of the adhesion strength parameter.** (A–C) Actin velocity map (A) minus substrate velocity map (B) gives the map of actin velocity with respect to the substrate (C). (D and E) A substrate deformation map (D) was used to calculate the stress map (E). (A–E) Arrows indicate the direction and relative magnitude of velocity (A–C), deformation (D), and traction stress (E). (F) Map of actin velocity–stress alignment and cosine of the angle between F-actin velocity and stress vectors. (G) A map of adhesion strength was computed as a ratio of the stress map and the map of actin velocity with respect to the substrate. The contour within the cell corresponds to the region of the opposite alignment of actin velocity and stress, which is shown in blue in F. (H) The analysis of adhesion strength dynamics in a cell that changed direction of motion showed a drop in adhesion strength upon detachment at one side of the cell (at 20 s) and its subsequent recovery (Video 2). (A–H) The cell margin is shown with the white outline. (I) Coupling in 120-μm^2 areas (approximately one quarter of the cell) at the two sides of the cell shown in H was quantified as a fraction of the area in which coupling exceeded 1 kPa s/μm. Resulting values for the left and right sides and their ratio (left to right) are plotted (left, right, and ratio are measured in nondimensional units on the left scale) versus time along with the cell turn angle (direction change is measured in degrees on the right scale). Cell turn angle was measured as the difference between the orientations of the cell's long axis (determined by approximating the cell with an ellipse) in each pair of the sequential frames. Time is indicated in the images. Bars, 10 μm.

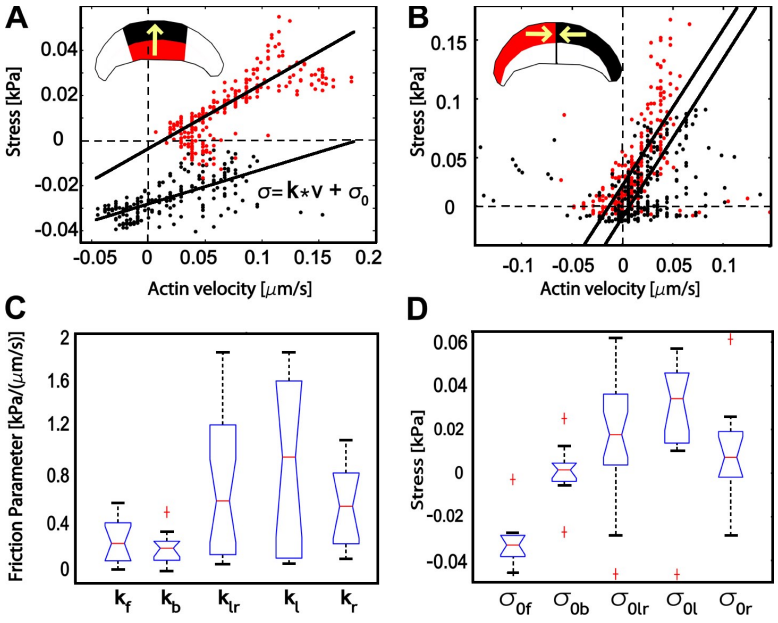

Figure 3. **Analysis of the relationship between stress and actin velocity.** (A) Plot of forward projection of the stress versus forward projection of F-actin speed for all positions in the central region of the cell. Positions within the front half of this region are shown in black, and positions within the back half are shown in red. The inset shows boundaries of the central region, its subdivision into the front and back halves, and the direction to which velocity and stress were projected (arrow). (B) Plot of lateral projection of stress versus lateral projection of F-actin velocity for all positions in the frontal region of the cell. Positions on the left from the cell symmetry axis are shown in red, and positions on the right of it are shown in black. A positive sign was assigned to centripetal velocity and stress. The inset graphic is as in A. Each cloud in A and B was fitted using the least squares method with a linear function $\sigma = k\,v + \sigma_0$, where k is the slope and σ_0 is a constant. (C) Box plots of k for the data corresponding to the forward stress at the front (k_f) and the back (k_b) of the cell and the lateral centripetal stress for the left and right halves of the cell mixed together (k_{lr}), the left (k_l), and the right (k_r) halves of the cell. (D) Box plots of σ_0 for the data corresponding to forward stress at the front (σ_{0f}), the back (σ_{0b}), the left and right mixed together (σ_{0lr}), the left (σ_{0l}), and the right (σ_{0r}). Box and whisker plots in all figures indicate the 25% (lower bound), median (middle line), and 75% (upper bound) nearest observations within 1.5 times the interquartile range (whiskers), 95% confidence interval of the median (notches), and outliers (+). The analysis of front–back and lateral components of actin velocity and stress was performed for 12 matched pairs of velocity and stress maps that were derived from video sequences of five different migrating cells.

rotate at a lower rate while the coupling asymmetry fluctuated and then gradually decreased (Fig. 2, H and I). A likely interpretation of this dynamic sequence is that when coupling of the actin network to the substrate weakened at the cell's right side, the actin movement at this side had to accelerate to balance propulsive and resisting traction stresses at the front and left side of the cell. This led to partial detachment and a left turn of the cell. Initial changes in the distribution of traction stress and the actin velocity pattern were not dramatic when considered separately (unpublished data). It is their ratio, the coupling coefficient, that provided an early indication of the change of cell behavior.

Separation of gripping and slipping contributions to the force transmission mechanism

The lack of alignment of actin velocity and traction stress vectors in the central region of the cell indicated that the coupling coefficient defined in the previous section has limited applicability as a tool to quantify actin–substrate interaction. One reason for misalignment of the stress and actin motion could be that the actin network is mechanically anisotropic and transmits the force in some directions better than in others. Another possibility is that transmission of the force to the substrate may be partially or completely independent of the velocity of actin motion. One could imagine that if the actin network were under tension from within the cell and in a stable, gripping connection to the extracellular matrix, this tension could be transmitted to the substrate without movement of the actin network. To investigate the possible anisotropy of the force transmission and to isolate velocity-dependent (slipping) and -independent (gripping) components of the traction, we analyzed the dependence of traction stress on actin velocity in specific regions of the cell and along specific directions. Cell regions were selected wherein the behavior of actin velocity and stress was relatively uniform. Fig. 3 A shows a plot of the projections of the local traction stress along the direction of the cell's motion (termed forward direction from here on) versus forward projections of actin velocity in the central region of the cell. The central region was selected because the predominant direction of actin velocity and traction stress in this region was along the front–back axis. The region was further subdivided as shown in the inset of Fig. 3 A into approximately equal front (black) and back (red) parts. Experimental points corresponding to these two parts (shown in matching colors in Fig. 3 A) formed two well-separated, elongated clouds. Both clouds exhibited an overall positive slope, indicating that the traction stress generally increased with actin velocity. This is as expected for a slipping or frictional type of force transmission. However, although the cloud representing the back of the cell intersected the stress axis at zero, the stress at the cell front was negative (backward oriented) at zero actin velocity, suggesting a velocity-independent propulsive stress component. To quantify velocity-dependent (frictional) and -independent stress contributions, each cloud was fitted using the least squares method with a linear function $\sigma = k\,v + \sigma_0$, where σ is stress, v is actin velocity, k is a coefficient of proportionality between stress and velocity, and σ_0 is a component of stress independent of velocity. k could be considered a parameter describing friction between the slipping actin network and the substrate, whereas σ_0 represents part of the stress transmitted through gripping of the actin network to the substrate. In the following sections, we will refer to k as a friction parameter and to σ_0 as gripping stress.

The fits represented on Fig. 3 A indicate that velocity-independent gripping stress contributed significantly to the propulsive traction at the front of the cell but that the resisting traction at the back of the cell was generated almost entirely by a frictional slippage. This result suggests that the mechanisms of force transmission were different at the front and back of the cell, reflecting cell polarization.

Similar analysis was performed for the components of stress and velocity normal to the direction of cell locomotion (termed lateral components in the following sections). For the analysis of lateral components, we selected a wide zone encompassing approximately half of the cell from its front edge to the middle and from its left to its right extremity. The reason for excluding the back part of the cell from the analysis was that actin lateral velocity often exhibited large fluctuations at the back of the cell. The front part of the cell was further subdivided symmetrically into left and right halves, which were analyzed separately. The clouds of experimental points corresponding to left and right halves of the front zone exhibited significant overlap (Fig. 3 B). This is not surprising because keratocytes are generally symmetric around the front–back axis, and the right and left halves of the cell are expected to be equivalent. We fitted the lateral stress–velocity plots with linear function and determined the friction parameter and a gripping stress component as described at the beginning of this section.

The analysis of forward and lateral stress and velocity components was performed in a total of 12 matched pairs of velocity and stress maps that were derived from video sequences of five different migrating cells. The mean values of the friction parameter and gripping stress are represented in Fig. 3 (C and D). The majority of maps revealed significant backward-oriented gripping stress at the front of the cell, whereas the stress at the back of the cell was almost entirely frictional (gripping stress at the front was statistically different from that at the back, whereas gripping stress at the back was no different from zero at the 95% confidence level). The friction parameters for the forward stress component at the front and back of the cell were not different at the 95% confidence level, but the friction parameter for the lateral stress (left and right halves of the cells lumped into one group) was significantly higher than the friction parameter for the forward stress component at the 95% confidence level. The gripping component of the lateral stress was small with respect to the total traction stress at the cell sides but, at the 95% confidence level, exhibited statistically significant orientation toward the cell center, which is consistent with elastic tension generation between the lateral flanks of the cell. Friction parameters and gripping components of the lateral stress analyzed separately at the left and right halves of the cell were not statistically different, as expected, providing a test for the consistency of the analysis. In summary, detected differences in friction parameter and gripping stress indicate that different parts of the cell transmit cytoskeletal forces to the substrate in different ways: propulsive (backward) traction stress at the cell front is largely contributed by the gripping of the actin network to the substrate, whereas high lateral traction stress at the cell sides is maintained as a result of high friction between a slipping actin network and the substrate in the lateral direction.

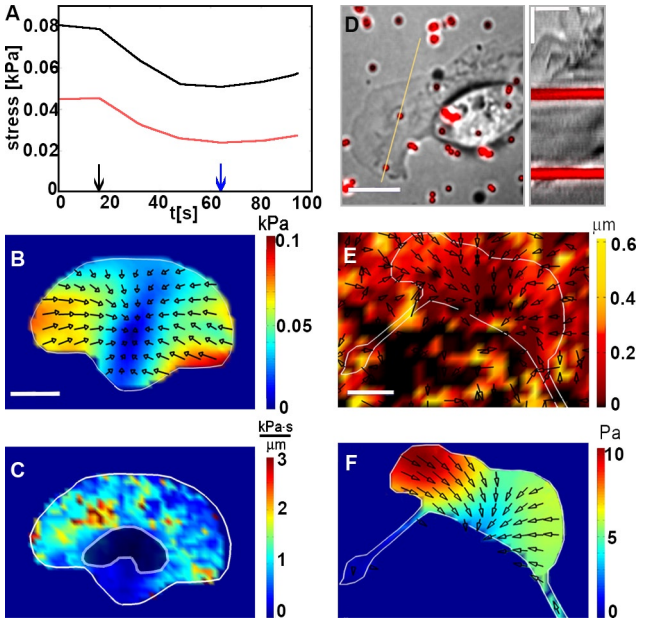

Figure 4. **Contribution of actin assembly and actomyosin contraction to the traction stress and actin–substrate coupling.** (A) Evolution of the 90th percentile (black line) and the mean stress (red line) after the addition of 2 μM cytochalasin D. Arrows indicate the time of addition of cytochalasin D (black) and the time of the arrest of the leading edge (blue). (B and C) The stress map (B) and actin–substrate coupling map (C; dark area shows negative correlation between actin velocity and stress as in Fig. 2 G) of cytochalasin D–treated cell at the time of the arrest of the leading edge (Video 3) are similar to the ones of control cells (see Fig. 2, E–G). (D) Brightfield image (gray) of the cell migrating at 30 min after the addition of 50 μM blebbistatin superimposed on a fluorescent image (red) of gelatin substrate with 0.5-μm latex beads. One frame of the image sequence is shown on the left, and a kymograph generated along the yellow line in the image is shown on the right. No bead movement is detectible in the kymograph. For the kymograph: vertical bar, 5 μm; horizontal bar, 60 s. (E and F) The substrate deformation field (E) and computed stress field (F) for the blebbistatin-treated cell that developed an extended tail. (B, C, E, and F) The cell margin is shown with the white outline. (B, E, and F) Arrows indicate the direction and relative magnitude of the traction stress (B and F) and substrate deformation (E). Bars, 10 μm.

Contribution of actin assembly and actomyosin contraction to the forces transmitted to the substrate

To evaluate contributions of actin assembly and actomyosin contraction to the forces transmitted to the substrate, we treated the cells with the inhibitor of actin assembly cytochalasin D and with the inhibitor of actin–myosin interaction blebbistatin. As expected, application of cytochalasin D resulted in the arrest of protrusion at the leading edge of the cell within a few minutes after addition of the drug. Fig. 4 A shows the dynamics of the 90th percentile and mean substrate stresses during cytochalasin D treatment. A decrease in the stress was observed, but the cell continued to apply significant stress (65% of the value before treatment) after the protrusion at the leading edge stopped. The stress and actin–substrate coupling maps after the arrest of protrusion (Fig. 4, B and C; and Video 3) were similar to those obtained for cells not treated with cytochalasin D, with the only notable difference being that the regions of laterally oriented stress at the cell flanks were proportionally larger. This difference could reflect the lateral contraction of the central part of

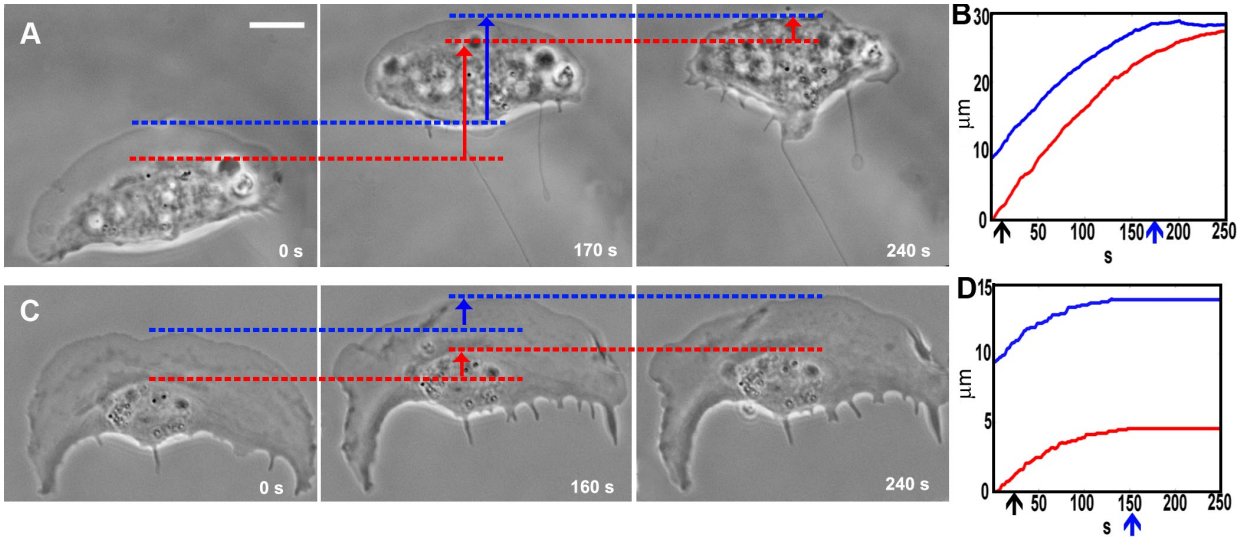

Figure 5. **Translocation of the cell body depends on leading edge protrusion in blebbistatin-treated cells.** (A and B) Treatment of the cell with cytochalasin D results in the arrest of the leading edge while the cell body continues to move (Video 4, left). (C and D) Treatment with cytochalasin D of the cell pretreated with blebbistatin results in the simultaneous arrest of the leading edge and the cell body (Video 4, right). (A and C) Time-lapse sequences of phase-contrast images; experiment on a clear glass substrate is shown for clarity, but similar results were obtained on elastic gelatin substrate. Blue and red lines and arrows indicate the positions and displacements of the leading edge and the front margin of the cell body, respectively; time after the addition of cytochalasin D is indicated in the images. (B and D) Displacement in time of the leading edge (blue) and of the front margin of the cell body (red). The time of cytochalasin D addition is indicated by black arrows, and blue arrows indicate the time when the front of the cell stopped. Stress dynamics during comparable cytochalasin D treatment are shown in Fig. 4 (A–C). Stress dynamics during combined blebbistatin and cytochalasin D treatment were not reliably measurable because of the low level of deformation. Bar, 10 µm.

the cell upon addition of the drug. Thus, a significant part of the forces applied by the cell to the substrate and the overall pattern of their transmission were independent of actin assembly.

Consistent with an earlier study (Schaub et al. 2007), treatment with blebbistatin resulted in a decrease of the velocity and frequently in fragmentation of the cells; however, many cells continued to migrate. 30 min after the application of 50 µM of the drug, most of the migrating cells did not produce any detectable deformation of the substrate (evident from the kymograph in Fig. 4 D). Note that substrate deformation was always readily detectable in the same experiment before blebbistatin treatment. Some movement of the substrate in blebbistatin-treated cells was detected in the cases in which cells developed long, stretched tails (Fig. 4 E). These deformations and the corresponding traction stresses (the maximum stress value, 10 Pa and 90th percentile, 9.3 Pa for the cell shown in Fig. 4 F) were ~5–10 times smaller than in the cells not treated with blebbistatin. Because deformations were at the limit of detection, the computed traction map should be considered an estimation of the overall traction stress magnitude rather than reliable information about its local distribution. A lower concentration of blebbistatin (25 µM) produced a similar effect, but it took longer (~1 h) for an equivalent reduction of the traction stress to develop, whereas a higher concentration of the drug (100 µM) induced fast fragmentation of the majority of cells (unpublished data). Dramatic reduction of the substrate stress upon inhibition of myosin activity suggests that most of the forces applied by a migrating cell to the substrate depended on actomyosin contraction. Despite the drop in force production, the cells that remained intact and migrated showed a range of actin velocity similar to control cells (Schaub et al. 2007; unpublished data). Actin–substrate coupling maps were not computed for blebbistatin-treated cells, but the dramatic reduction in substrate stress and the similarity of actin velocity to control values indicated significant reduction in the coupling coefficient.

Dual mechanism of cell translocation

We asked whether the mechanism of cell translocation in the cells treated with blebbistatin was different from the one in untreated cells. Previously, it was shown (Anderson et al., 1996) that translocation of the cell body in keratocytes was partially independent from actin assembly at the front: after the arrest of front protrusion upon application of cytochalasin D, the cell body continued to move, suggesting that a mechanism other than actin assembly powered retraction of the rear and translocation of the cell body.

We confirmed that in the cells not treated with blebbistatin, translocation of the cell body persisted after the arrest of front protrusion by cytochalasin D (Fig. 5, A and B; and Video 4, left): after the front stopped, the back of the cell continued to move until the front margin of the cell body reached the leading edge of the lamellipodium. The residual cell body translocation was likely powered by actomyosin-dependent traction stresses that we registered in cytochalasin D–treated cells (Fig. 4 B). These forces pulled the cell body as far as the lamellipodial actin network extended.

Cytochalasin D similarly induced the arrest of the front protrusion in blebbistatin-treated cells. Despite the fact that blebbistatin-treated cells migrated more slowly than control cells, the kinetics of the cytochalasin D–induced protrusion arrest was similar in both cases (half-time of the arrest was ~40–50 s), suggesting that the drug similarly inhibited actin

assembly. However, the effect on cell body motion was different. In contrast to the control cells, the addition of cytochalasin D to blebbistatin-treated cells resulted in the nearly synchronous reduction of the velocity and eventual simultaneous arrest of the leading edge and the cell body. No residual movement of the cell body was observed after the stop of the front. Fig. 5 (C and D) and Video 4 show the kinetics of the front and cell body movement on the rigid glass substrate (selected for image clarity), but similar results were obtained on elastic gelatin substrata. Thus, in blebbistatin-treated cells, the movement of the cell body was tightly coupled to the protrusion of the front. These results suggest that translocation of the cell body could be powered by either of the two redundant mechanisms, actomyosin contraction or actin assembly.

Discussion

In this study, we have for the first time analyzed the relationship between the motion of the actin network and generation of the traction force over the entire cell in the process of rapid persistent migration. To quantify the efficiency of the force transmission from the actin network to the substrate, we introduced a new parameter termed a coefficient of actin–substrate coupling. This parameter is based on the assumption of a linear relationship between traction and actin network velocity in which the coupling coefficient is the proportionality constant. Maps of actin–substrate coupling represent a simple way to quantify differences in force transmission efficiency between different cell regions. According to these maps, coupling of the actin network to the substrate was generally tight under the leading lamellipodium and lateral flanks of the cell and weak under the trailing cell body. Coupling maps were also reliable indicators of the changes in cell motion behavior, e.g., turns. Actin–substrate coupling as defined in this study may be a convenient parameter to use in quantitative modeling of cell motility, with results that could be directly compared with the experimental data (Rubinstein et al., 2009).

We have also identified the limitations of the coupling parameter, which stem from the fact that the orientation of the stress vector did not always coincide with that of the actin velocity vector. To overcome these limitations, we have further investigated the relationship between actin velocity and traction stress in the specific regions of the cell and along specific directions. This analysis revealed that two different mechanisms underlay the tight coupling between actin and the substrate observed at the front and flanks of the cell: at the front, the stress was transmitted in a manner partially independent of actin velocity, indicating gripping of the actin network to the substrate, whereas at the cell flanks, efficient force transmission was largely the result of high friction between a slipping actin network and the substrate. At the cell body, relatively low friction in combination with the absence of gripping stress transmission accounted for an overall ineffective coupling of the actin network to the substrate. Thus, our results indicate that depending on the cell region, the adhesions could transmit cytoskeletal forces in different ways: through a purely frictional slippage or at least partially through gripping to the substrate in a velocity-independent way. Additionally, frictional resistance of the adhesions may be cell region and/or orientation specific as indicated by the differences in the friction parameter between forward and lateral directions.

These results are consistent with a few recent studies suggesting different functional modes of adhesion. Jurado et al. (2005) reported indirect evidence that adhesions could function in two different modes (slipping or gripping) in slowly and rapidly moving keratocytes. More recently, Gardel et al. (2008) and Chan and Odde (2008) demonstrated different functional adhesion modes in epithelial and neuronal cells, with transitions depending on actin velocity and substrate rigidity, respectively. Both cell types are characterized by relatively slow protrusion and fast retrograde flow at the periphery. The analysis of traction stress transmission was performed only in peripheral regions of these cells. Our study is the first to correlate actin motion to traction stress over the entire rapidly migrating cell. The implications of our results in the context of the overall polarity of migrating cells are that propulsive tractions at the cell front are at least partially generated in an actin velocity–independent manner, through gripping to the substrate, whereas resistive traction of the trailing cell body is caused entirely by frictional slippage. One can further speculate that a separation of velocity-dependent and -independent stresses is essential to defining the steady-state velocity of the cell. Indeed, tension generated by the cytoskeleton is applied between gripping front lamellipodium and a slipping cell body. As a result, a cell body is expected to accelerate until frictional resisting traction at the back balances cytoskeletal tension. After this point, the cell body translocation would proceed at a constant velocity. Note that at a steady-state, this velocity is matched by the rate of actin assembly at the cell front. How the cell body translocation rate feeds back to the actin assembly rate at the front is as yet unclear and represents a major challenge for future studies.

What are the mechanisms of switching between the velocity-independent (gripping) and frictional (slipping) modes of the force transmission at the adhesion sites? Gardel et al. (2008) suggested that actin velocity plays a critical role. However, it is not clear whether the biphasic adhesion behavior reported in this paper is equivalent to adhesion modes identified in our study. The inverse correlation of the traction stress to actin velocity observed by Gardel et al. (2008) at the cell periphery may represent progressive engagement of the adhesions working in a slipping mode, which would result in the increase in the effective friction and a slowing down of the actin network. An adjacent zone of direct correlation between actin velocity and stress may correspond to the constant friction associated with mature adhesions. In contrast to this study, we did not find a biphasic relationship between actin velocity and traction stress. Instead, stress increased rather monotonously with actin velocity in all cell regions. The highest stress was observed under cell flanks in which actin velocity was generally over 50 nm/s, which is well above the critical velocity value identified by Gardel et al. (2008) as corresponding to the peak of the stress. Given the overall very regular and smooth deformation and stress patterns displayed by steady-state migrating keratocytes, it is unlikely that any biphasic stress behavior remained undetected and could

be revealed by means of increasing the resolution of stress mapping. We conclude that the maturation of adhesions themselves is more likely than the actin velocity to control the switch between gripping and slipping force transmission modes. One possibility, analogous to how Chan and Odde (2008) suggested that the switch in neuronal filopodia adhesion depends on substrate stiffness, is that the transition to the slipping transmission mode is controlled by the age-dependent stiffening of the adhesion itself. Younger adhesions could be expected to be more elastic and to grip more effectively than the older ones.

The idea of a maturation-dependent switch in adhesion mode is consistent with previous protein localization and dynamics studies in keratocytes. This earlier work demonstrated small adhesion complexes distributed rather uniformly under the lamellipodium and the cell body and larger adhesions at the sides of the cell (Lee and Jacobson, 1997; Anderson and Cross, 2000). Older adhesions under the cell body and cell flanks are expected to act in a largely frictional mode, with larger adhesions under the cell flanks providing higher frictional resistance.

In the second part of our study, we investigated the contributions of different sources of traction stress to the overall mechanism of cell migration. Although inhibition of actin assembly only moderately affected cell traction, the blocking of myosin activity with blebbistatin resulted in a very dramatic drop in the magnitude of the traction stress. Nevertheless, some of the blebbistatin-treated cells continued to migrate persistently. Translocation of the cell body in these cells was fully dependent on actin assembly at the front, whereas in the cells with functional myosin II, cell body translocation occurred in a manner partially autonomous from actin assembly. Based on these results, one could hypothesize that cell translocation can proceed in two different modes (Fig. 6). When myosin II is active, the cell develops relatively strong adhesions with the substrate, and actomyosin contraction results in strong tension between the leading edge and the cell body (Fig. 6, top, dark arrows), which is transmitted to the substrate in the form of a strong propulsive and resisting traction. Adhesion at the front transmits cytoskeletal tension in a gripping manner (front adhesions are schematically shown in Fig. 6 as having straight "teeth" gripping to the matching pits in the extracellular matrix), whereas the back and side adhesions exhibit frictional slippage (inclined teeth slipping out of matrix and higher frictional parameter at the sides than at the back). Adhesion asymmetry promotes retraction at the back, thus contributing to the directionality of the cell motion. The cell moves in an "all-wheel drive" mode generating forces both at its front and rear: actin assembly pushes the front forward and creates a new actin network for myosin II to pull on, whereas myosin-powered contraction serves to break resisting adhesions at the back and sides of the cell and drives the cell body movement in partial autonomy from the front protrusion.

When myosin II is inhibited, the cell switches to a "front-wheel only" drive mode (Fig. 6, bottom). In this case, cell translocation is tightly coupled to the front protrusion, suggesting that forces are generated by actin assembly at the front only, whereas the cell rear moves passively. Relatively weak protrusive forces (Bohnet et al., 2006; Brunner et al., 2006; Prass et al., 2006)

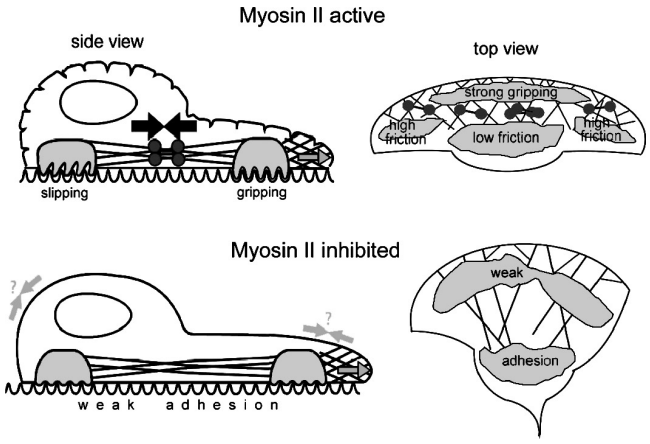

Figure 6. **Diagram of the force generation and transmission in migrating cells.** Active myosin II (dumbbell figures in the top schemas) generates tension between the front and the back of the cell, which is transmitted to gripping adhesions (straight teeth) at the front and slipping adhesions (tilted teeth) at the back and sides. When myosin II is inhibited (bottom schemas), the pushing force of actin assembly at the front is transmitted to the back, likely through the plasma membrane or the cortical cytoskeleton (gray arrows and question mark). The adhesions are weak (shallow teeth), allowing the cell to move without transmitting significant force to the substrate.

at the front may be sufficient to power the motion of the whole cell because the cell is weakly adherent to the substrate (Fig. 6, bottom, shallow adhesion teeth) and does not have to generate strong propulsive traction to overcome resisting adhesive forces. A plasma membrane (Keren et al., 2008) or some passive cytoskeletal element (e.g., submembranous cortical cytoskeleton) could serve as a mechanical link transmitting the force from the front to the back of the cell (Fig. 6, bottom, gray arrows). If the force-transmitting element is indeed the plasma membrane, one could expect it to be stretched in blebbistatin-treated cells (Fig. 6, bottom, smooth membrane) and loose in control cells (Fig. 6, top, wrinkled membrane). Because the protrusion force is relatively weak, the myosin-independent mode of motion is expected to be perturbed easily by similarly small forces arising from, e.g., fluctuations of adhesion strength, encounters with mechanical obstacles, etc. The formation of extended tails, cell fragmentation, and the eventual arrest of migration in the presence of blebbistatin (Csucs et al., 2007; Schaub et al., 2007) may be a manifestation of this instability of motion. In the in vivo setting, cell motion and pathway finding within tissue are likely to be obstructed by significant barriers and may rely on myosin-powered contraction to overcome these obstacles (Lämmermann et al., 2008).

In summary, our correlative study of cytoskeletal dynamics, force generation, and cell motion uncovered different polarization-related modes of adhesive machinery, identified redundant driving forces for cell translocation, and provided quantitative information on cell adhesion for forthcoming models of cell migration. Different modes of adhesion machinery may have important implications not only for the polarization of migrating cells but also for mechanical sensing and tissue pattern formation. Identification of the molecular mechanisms of spatial adhesion control and front–back coordination in polarized cells remains the major challenge for the future.

Materials and methods

Cell culture and microscopy

Black tetra (*Gymnocorymbus ternetzi*) epidermal keratocytes were cultured as described previously (Schaub et al., 2007), detached from the glass substrate with a 0.25% trypsin-EDTA solution (0.1 ml per 22 × 22 mm^2 coverslip; Sigma-Aldrich), suspended in 0.4 ml of culture medium, and transferred to a gelatin substrate. Phase-contrast, brightfield, and fluorescence microscopy were performed using an inverted microscope (Eclipse TE300; Nikon) with a 60× NA 1.4 Plan objective and a cooled charge-coupled device camera (Micromax 1024BFT; Roper Industries) operated with MetaMorph software (Universal Imaging). Brightfield rather than phase-contrast microscopy was used to minimize distortion of the image in the presence of large 0.5-µm solid latex beads on the gelatin substrate. Two-color fluorescent image sequences were obtained by sequential excitation of fluorescence in red and green channels with a time interval of 2.5 s (5 s between sequential images in each single channel).

Gelatin substrate preparation and calibration

The gelatin substrata were manufactured and calibrated as described by Doyle and Lee (2002). In brief, 500 µl of 5% gelatin (Dr. Oetker) dissolved in distilled water was allowed to solidify at 4°C before adding 0.2 µm FITC-labeled or 0.5 µm TRITC-labeled microspheres (Polysciences, Inc.) at a 1:100 dilution in distilled water. Then the lower layer of gelatin was liquefied and removed to obtain an ∼40-µm thick substrate with a thin layer of fluorescent beads at its top. The gelatin was calibrated by bead indentation (steel ball of 0.9 mm in diameter; density, 15.26 g/cm^3) using the Hertz's low that allows to compute the Young's Modulus from the weight of the beads, its diameter, and the depth of the indentation. The Young's Modulus for 5% gelatin substrata used in this study was ∼6 kPa.

Microinjection

Cells were microinjected on the gelatin substrate with Alexa Fluor 568–phalloidin (Invitrogen) dissolved at a concentration of 2–4 µg/ml in 15% dimethyl sulfoxide as described previously (Schaub et al., 2007).

Velocity and stress maps

Actin and substrate velocity maps were obtained using a MatLab (MathWorks) tracking routine (Schaub et al., 2007) based on correlation between small regions of the image. The images were resized with interpolation to 200% and segmented in square regions with dimensions of 65 × 65 $pixels^2$ (3.5 × 3.5 $µm^2$) that partially overlapped (the distance between adjacent regions was 20 pixels). Each region was compared with regions shifted with respect to its original position by a distance of up to 30 pixels in the subsequent image of the time-lapse sequence.

Images of the undeformed substrate were taken before or after the cell passage or after removal of the cell from the substrate with a micropipette. Deformation maps were obtained by tracking motion of the beads between the undeformed and deformed state with the same algorithm that was used for velocity mapping.

A map of the stress exerted by the cell on the substrate was obtained from the substrate deformation using the data inversion method described in Ambrosi (2006) and previously applied to determine traction patterns in other contexts (Ambrosi et al., 2009). The basic idea of the method dates back to the seminal work by Dembo and Wang (1999). The originality of the approach is that data are inverted on the basis of a finite element solution of the elastic stress field and not by direct convolution of the corresponding Green functions. Variational calculus applied to classical Tichonov regularization yields a system of differential equations in which the unknowns are the displacement field very near to the experimental one and the shear stress. The algorithm is based on an approximate solution of the elasticity problem. The elastic stress field is searched for among the null mean fields that are admissible at the equilibrium. The algorithm has been successfully compared with classical methods with very similar results while being computationally much faster.

As usual in inverse problems, the regularization procedure is needed to damp high frequency components of the experimental errors; this procedure involves an arbitrary cutoff that is reflected in the choice of a scalar parameter (ε in the aforementioned papers). The results shown in the present paper are poorly dependent on the choice of such a parameter in a range that corresponds to filter wavelengths below 1/10 the length of the cell. To compute the ratio of the stress to actin velocity (adhesion strength parameter) and to produce the stress–velocity plots (Fig. 3), the actin velocity map and the stress map were interpolated onto the common grid.

Cytoskeletal inhibitors

2 µM cytochalasin D (Sigma-Aldrich) and 50 µM blebbistatin (EMD) were used to inhibit actin assembly and myosin II activity, respectively.

Online supplemental material

Video 1 shows actin motion and substrate deformation in fish keratocyte migrating over gelatin substrate with fluorescent beads. Video 2 shows the dynamics of friction in a keratocyte that changes direction of motion. Video 3 shows the dynamics of stress and friction after the arrest of the leading edge in a keratocyte treated with cytochalasin D. Video 4 shows the kinetics of migration arrest in a keratocyte treated with cytochalasin D and a keratocyte pretreated with blebbistatin and treated with cytochalasin D. Online supplemental material is available at http://www.jcb.org/cgi/content/full/jcb.200906139/DC1.

We are grateful to Sebastien Schaub for the help in using his motion-tracking algorithm and to Alex Mogilner for critical discussion and suggestions.

This work was supported by Swiss National Science Foundation grant 3100A0-112413.

Submitted: 22 June 2009
Accepted: 21 December 2009

References

Ambrosi, D. 2006. Cellular traction as an inverse problem. *SIAM J. Appl. Math.* 66:2049–2060. doi:10.1137/060657121

Ambrosi, D., A. Duperray, V. Peschetola, and C. Verdier. 2009. Traction patterns of tumor cells. *J. Math. Biol.* 58:163–181. doi:10.1007/s00285-008-0167-1

Anderson, K.I., and R. Cross. 2000. Contact dynamics during keratocyte motility. *Curr. Biol.* 10:253–260. doi:10.1016/S0960-9822(00)00357-2

Anderson, K.I., Y.L. Wang, and J.V. Small. 1996. Coordination of protrusion and translocation of the keratocyte involves rolling of the cell body. *J. Cell Biol.* 134:1209–1218. doi:10.1083/jcb.134.5.1209

Beningo, K.A., K. Hamao, M. Dembo, Y.L. Wang, and H. Hosoya. 2006. Traction forces of fibroblasts are regulated by the Rho-dependent kinase but not by the myosin light chain kinase. *Arch. Biochem. Biophys.* 456:224–231. doi:10.1016/j.abb.2006.09.025

Bohnet, S., R. Ananthakrishnan, A. Mogilner, J.J. Meister, and A.B. Verkhovsky. 2006. Weak force stalls protrusion at the leading edge of the lamellipodium. *Biophys. J.* 90:1810–1820. doi:10.1529/biophysj.105.064600

Brunner, C.A., A. Ehrlicher, B. Kohlstrunk, D. Knebel, J.A. Käs, and M. Goegler. 2006. Cell migration through small gaps. *Eur. Biophys. J.* 35:713–719. doi:10.1007/s00249-006-0079-1

Chan, C.E., and D.J. Odde. 2008. Traction dynamics of filopodia on compliant substrates. *Science*. 322:1687–1691. doi:10.1126/science.1163595

Chen, C.S., J. Tan, and J. Tien. 2004. Mechanotransduction at cell-matrix and cell-cell contacts. *Annu. Rev. Biomed. Eng.* 6:275–302. doi:10.1146/annurev.bioeng.6.040803.140040

Cramer, L.P. 1997. Molecular mechanism of actin-dependent retrograde flow in lamellipodia of motile cells. *Front. Biosci.* 2:d260–d270.

Csucs, G., K. Quirin, and G. Danuser. 2007. Locomotion of fish epidermal keratocytes on spatially selective adhesion patterns. *Cell Motil. Cytoskeleton*. 64:856–867. doi:10.1002/cm.20230

Dembo, M., and Y.L. Wang. 1999. Stresses at the cell-to-substrate interface during locomotion of fibroblasts. *Biophys. J.* 76:2307–2316. doi:10.1016/S0006-3495(99)77386-8

Doyle, A.D., and J. Lee. 2002. Simultaneous, real-time imaging of intracellular calcium and cellular traction force production. *Biotechniques*. 33:358–364.

Galbraith, C.G., and M.P. Sheetz. 1999. Keratocytes pull with similar forces on their dorsal and ventral surfaces. *J. Cell Biol.* 147:1313–1324. doi:10.1083/jcb.147.6.1313

Gardel, M.L., B. Sabass, L. Ji, G. Danuser, U.S. Schwarz, and C.M. Waterman. 2008. Traction stress in focal adhesions correlates biphasically with actin retrograde flow speed. *J. Cell Biol.* 183:999–1005. doi:10.1083/jcb.200810060

Geiger, B., and A. Bershadsky. 2002. Exploring the neighborhood: adhesion-coupled cell mechanosensors. *Cell*. 110:139–142. doi:10.1016/S0092-8674(02)00831-0

Heidemann, S.R., and R.E. Buxbaum. 1998. Cell crawling: first the motor, now the transmission. *J. Cell Biol.* 141:1–4. doi:10.1083/jcb.141.1.1

Hu, K., L. Ji, K.T. Applegate, G. Danuser, and C.M. Waterman-Storer. 2007. Differential transmission of actin motion within focal adhesions. *Science*. 315:111–115. doi:10.1126/science.1135085

Iwadate, Y., and S. Yumura. 2008. Actin-based propulsive forces and myosin-II-based contractile forces in migrating *Dictyostelium* cells. *J. Cell Sci.* 121:1314–1324. doi:10.1242/jcs.021576

Jurado, C., J.R. Haserick, and J. Lee. 2005. Slipping or gripping? Fluorescent speckle microscopy in fish keratocytes reveals two different mechanisms for generating a retrograde flow of actin. *Mol. Biol. Cell*. 16:507–518. doi:10.1091/mbc.E04-10-0860

Keren, K., Z. Pincus, G.M. Allen, E.L. Barnhart, G. Marriott, A. Mogilner, and J.A. Theriot. 2008. Mechanism of shape determination in motile cells. *Nature*. 453:475–480. doi:10.1038/nature06952

Lämmermann, T., B.L. Bader, S.J. Monkley, T. Worbs, R. Wedlich-Söldner, K. Hirsch, M. Keller, R. Förster, D.R. Critchley, R. Fässler, and M. Sixt. 2008. Rapid leukocyte migration by integrin-independent flowing and squeezing. *Nature*. 453:51–55. doi:10.1038/nature06887

Lee, J., and K. Jacobson. 1997. The composition and dynamics of cell-substratum adhesions in locomoting fish keratocytes. *J. Cell Sci.* 110:2833–2844.

Lee, J., A. Ishihara, and K. Jacobson. 1993. The fish epidermal keratocyte as a model system for the study of cell locomotion. *Symp. Soc. Exp. Biol.* 47:73–89.

Lo, C.M., D.B. Buxton, G.C. Chua, M. Dembo, R.S. Adelstein, and Y.L. Wang. 2004. Nonmuscle myosin IIb is involved in the guidance of fibroblast migration. *Mol. Biol. Cell*. 15:982–989. doi:10.1091/mbc.E03-06-0359

Lombardi, M.L., D.A. Knecht, M. Dembo, and J. Lee. 2007. Traction force microscopy in *Dictyostelium* reveals distinct roles for myosin II motor and actin-crosslinking activity in polarized cell movement. *J. Cell Sci.* 120:1624–1634. doi:10.1242/jcs.002527

Maciver, S.K. 1996. Myosin II function in non-muscle cells. *Bioessays*. 18:179–182. doi:10.1002/bies.950180304

Mitchison, T.J., and L.P. Cramer. 1996. Actin-based cell motility and cell locomotion. *Cell*. 84:371–379. doi:10.1016/S0092-8674(00)81281-7

Mogilner, A., and G. Oster. 2003. Polymer motors: pushing out the front and pulling up the back. *Curr. Biol.* 13:R721–R733. doi:10.1016/j.cub.2003.08.050

Oliver, T., M. Dembo, and K. Jacobson. 1999. Separation of propulsive and adhesive traction stresses in locomoting keratocytes. *J. Cell Biol.* 145:589–604. doi:10.1083/jcb.145.3.589

Pantaloni, D., C. Le Clainche, and M.F. Carlier. 2001. Mechanism of actin-based motility. *Science*. 292:1502–1506. doi:10.1126/science.1059975

Pollard, T.D., and G.G. Borisy. 2003. Cellular motility driven by assembly and disassembly of actin filaments. *Cell*. 112:453–465. doi:10.1016/S0092-8674(03)00120-X

Prass, M., K. Jacobson, A. Mogilner, and M. Radmacher. 2006. Direct measurement of the lamellipodial protrusive force in a migrating cell. *J. Cell Biol.* 174:767–772. doi:10.1083/jcb.200601159

Ridley, A.J., M.A. Schwartz, K. Burridge, R.A. Firtel, M.H. Ginsberg, G. Borisy, J.T. Parsons, and A.R. Horwitz. 2003. Cell migration: integrating signals from front to back. *Science*. 302:1704–1709. doi:10.1126/science.1092053

Rubinstein, B., M.F. Fournier, K. Jacobson, A.B. Verkhovsky, and A. Mogilner. 2009. Actin-myosin viscoelastic flow in the keratocyte lamellipod. *Biophys. J.* 97:1853–1863. doi:10.1016/j.bpj.2009.07.020

Schaub, S., S. Bohnet, V.M. Laurent, J.J. Meister, and A.B. Verkhovsky. 2007. Comparative maps of motion and assembly of filamentous actin and myosin II in migrating cells. *Mol. Biol. Cell*. 18:3723–3732. doi:10.1091/mbc.E06-09-0859

Smilenov, L.B., A. Mikhailov, R.J. Pelham, E.E. Marcantonio, and G.G. Gundersen. 1999. Focal adhesion motility revealed in stationary fibroblasts. *Science*. 286:1172–1174. doi:10.1126/science.286.5442.1172

Svitkina, T.M., A.B. Verkhovsky, K.M. McQuade, and G.G. Borisy. 1997. Analysis of the actin–myosin II system in fish epidermal keratocytes: mechanism of cell body translocation. *J. Cell Biol.* 139:397–415. doi:10.1083/jcb.139.2.397

Theriot, J.A., and T.J. Mitchison. 1992. Comparison of actin and cell surface dynamics in motile fibroblasts. *J. Cell Biol.* 119:367–377. doi:10.1083/jcb.119.2.367

Verkhovsky, A.B., T.M. Svitkina, and G.G. Borisy. 1999. Network contraction model for cell translocation and retrograde flow. *Biochem. Soc. Symp.* 65:207–222.

Vicente-Manzanares, M., M.A. Koach, L. Whitmore, M.L. Lamers, and A.F. Horwitz. 2008. Segregation and activation of myosin IIB creates a rear in migrating cells. *J. Cell Biol.* 183:543–554. doi:10.1083/jcb.200806030

Wang, Y.L. 2007. Flux at focal adhesions: slippage clutch, mechanical gauge, or signal depot. *Sci. STKE*. doi:10.1126/stke.3772007pe10.

Wessels, D., D.R. Soll, D. Knecht, W.F. Loomis, A. De Lozanne, and J. Spudich. 1988. Cell motility and chemotaxis in *Dictyostelium* amebae lacking myosin heavy chain. *Dev. Biol.* 128:164–177. doi:10.1016/0012-1606(88)90279-5

Yam, P.T., C.A. Wilson, L. Ji, B. Hebert, E.L. Barnhart, N.A. Dye, P.W. Wiseman, G. Danuser, and J.A. Theriot. 2007. Actin–myosin network reorganization breaks symmetry at the cell rear to spontaneously initiate polarized cell motility. *J. Cell Biol.* 178:1207–1221. doi:10.1083/jcb.200706012